Electronic Supplementary Information

Titania nanorods curve to lower their energy

Hengzhong Zhang *[a], Michael P. Finnegan [ab] and Jillian F. Banfield *[ac]

1. Synthesis of nanocrystalline titania

All synthesis chemicals, including titanium (IV) isopropoxide ($Ti[OCH(CH_3)_2]_4$) (99%, Sigma-Aldrich), absolute ethanol (>99.5 %, Sigma-Aldrich), hydrochloric acid (37 %, Sigma-Aldrich) and sodium hydroxide (> 97%, Sigma-Aldrich) were used as received.

Nanocrystalline titania was synthesized by the sol-gel method. A volume of 2.25 L deionized (DI) water was used as a solvent for synthesis and its pH was adjusted to 1.10 with 12 M HCl. The acidic solution was cooled to 4 – 6 ^{o}C in an ice bath. Then a solution containing 22.5 mL titanium isopropoxide and 225 mL ethanol was slowly dripped into the acidic solution undergoing magnetic stirring.

Titania precipitated from the solution as the liquid was evaporated in an 80°C oven. The obtained titania powder was then re-introduced into 100 mL DI water, forming a colloidal suspension with a pH of 2.05. Ions adsorbed on colloid particles were removed by dialysis. The titania colloid suspension was put into a dialysis tube made of a Spectra/Por (molecular weight cut off (MWCO) of 3500 Daltons) membrane, and was placed into a DI water bath under slow magnetic stirring. After changing the water in the bath four times, the colloid formed a gel, indicating that the pH of the colloid had risen to near the zero point of charge of the titania. The measured pH of the colloid in the dialysis tube and that of the water in the bath were both 5.2. This value is close to the pH_{ZPC} of titania reported in the literature.[1] The dialyzed titania was dried for two days at 30 $^{\circ}$C, yielding ~ 3 g powder of titania. The powder was further evacuated for one day using a Micromeritics ASAP 2010 gas adsorption instrument under a vacuum of 3 μm Hg pressure, and then kept in a desiccator for further use.

2. X-ray characterization of samples

The synthesized and hydrothermally treated titania samples were characterized by powder X-ray diffraction (XRD). About 0.5 mg of titania powder was dispersed with ethanol and then transferred to a low background single crystal quartz plate for diffraction. XRD patterns were collected using a Brukker Baker diffractometer (Cobalt target, 45 mV, 35 mA) in a 2θ range of 24 to 68° with a step size of 0.01° and a dwell time of 1 second at each step. Some patterns were collected using a PANalytical X'Pert PRO diffractometer (Cobalt target, 40 mV, 40 mA) in a 2θ range of 15 to 85° with a scanning rate of 1 ^{o}/min.

For XRD pattern of a sample, after fitting the Pearson VII functions to chosen XRD peaks, the full width at the half-maximum (FWHM) of each peak was obtained. The particle size of titania particles was calculated from the FWHM data (after correction for instrumental broadening) using the Scherrer equation with a Scherrer constant of 0.9. When more than one titania phase was present in hydrothermally treated samples, the integrated areas of anatase (101), brookite (121) and/or rutile (110) peaks were used to calculate the phase content using an analytical method developed previously. [2]

Figure S1 shows an XRD pattern of the synthesized sample. It shows that the synthesized sample is primarily anatase (with trace amount of brookite). The average particle size of anatase calculated using the (101) peak broadening is 3.6 nm, which is very close to those measured from TEM image (Fig. S2, below).

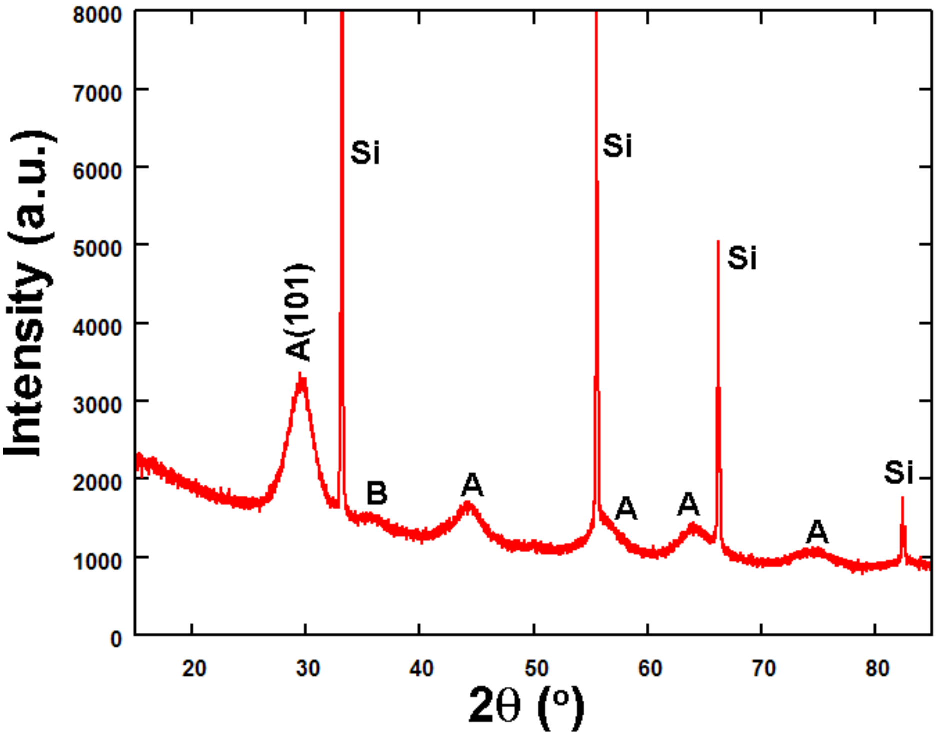

Fig. S1 XRD pattern of synthesized anatase sample (data collected using PANalytical X'Pert PRO). A trace amount of brookite (B) was present in the sample. A small amount of silicon (Si) powder (NIST SRM 640c) was used as an internal standard for accurate determination of 2θ angles and instrumental broadening.

3. Transmission electron microscope (TEM) and scanning electron microscopy (SEM) study of samples

The synthesized sample and chosen hydrothermally treated samples were examined with an ARM high-resolution TEM operated at 800 kV and a TopCon O2B 200 KV TEM. A small drop of powder-ethanol suspension was placed on a Formvar-coated copper TEM grid and dried naturally for imaging. The particle size, morphology, and crystallinity were determined.

Chosen hydrothermally processed samples were also examined using a high-resolution Hitachi S-5000 SEM for determination of size, morphology, and aggregation state of titania nanoparticles.

Figure S2 is a TEM image of synthesized anatase particles. Nanoparticles are close to spherical and are in a size range of 2 – 3 nm.

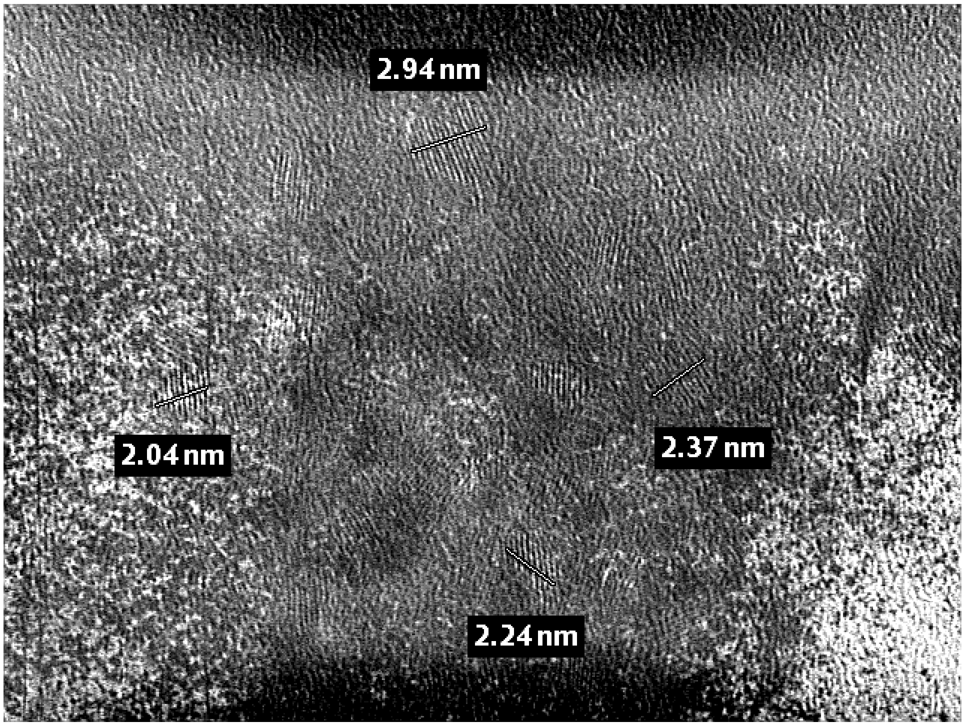

Fig. S2 TEM image of anatase nanoparticles synthesized by hydrolysis of titanium isopropoxide at 5 ^{o}C and pH 1. Measured sizes of several particles are shown.

4. Surface charges needed to bend an anatase nanorod

Assume that anatase nanorod bending is caused by electrostatic interactions of opposite surface charges distributed on the two terminals (ref. Fig. S3). Elastic energy is stored in the bent rod, which imparts a restoring or straightening force. At the bending/stretching equilibrium, the elastic force stretching the rod (f_e) is balanced by an opposite force (f'_e) stemming from the Coulombic force (f_c) acting upon the two oppositely charged terminals.

Suppose the rod has a cylinder-like geometry. The diameter is d, the curvature is R (radius), the distance between the two ends is L, the deflection of the bent rod is y, and half of the rod arc angle is ϕ (in radians). Then, the rod length is

$$L_r = 2\phi R \text{ (or } \phi = L_r/(2R)) \qquad \text{(S1)}$$

and

$$L = 2R\sin\phi \qquad \text{(S2)}$$

$$y = R(1 - \cos\phi) \qquad \text{(S3)}$$

The Coulombic force acting upon the two terminals is

$$f_c = K\frac{q^2}{L^2} \qquad \text{(S4)}$$

where $K = 9.0 \times 10^9$ Nm^2/C^2 is Coulomb's constant, and q is the quantity of the charge on either terminal. The force f'_e to balance the elastic force f_e is then

$$f'_e = f_c/\cos\phi = K\frac{q^2}{cos\phi L^2} \qquad (S5)$$

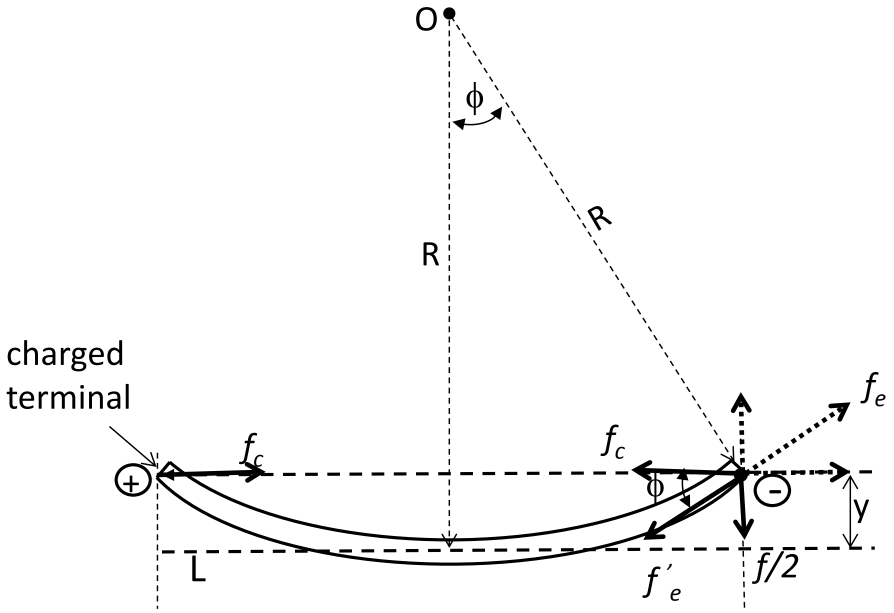

Fig. S3 Bending of an anatase nanorod introduces elastic energy that tends to straighten the rod. The elastic force stretching the rod (f_e) is balanced by an opposite force (f'_e) of the same magnitude whose horizontal component equals the Coulombic interaction force (f_c) due to charging of the two terminal surfaces.

The vertical component ($f/2$) of the force f'_e produces a total force f by the two ends, which acts vertically on the rod:

$$f = 2\tan\phi\, f_c \qquad (S6)$$

This force is equivalent to that required to bend a simply supported beam (a rod here).[3]

Inserting eq. S4 into eq. S6, one obtains

$$f = 2tan\phi K\frac{q^2}{L^2} \qquad (S7)$$

When this force is balanced by the elastic stretching, its quantity can be calculated using the geometric parameters and the elastic modulus (E) of the rod:[3]

$$f = \frac{3\pi E d^4 y}{4L^3} \qquad (S8)$$

Next, equate eq. S7 to eq. S8 and insert eqs. S2 and S3 into the resultant equation. After simplification and rearrangement, the surface charge density ($C_q = q/(\pi d^2/4)$ on a rod terminal is obtained:

$$C_q = \sqrt{\frac{3E(1-\cos\phi)}{\pi K \sin\phi \tan\phi}} \qquad \text{(S9)}$$

In a typical case, a bent rod has a length of ~ 80 nm (L_r), a diameter of ~ 10 nm (d), and a curvature of ~ 200 nm (R). Then, from eq. S1, $\phi = L_r/(2R) = 80/(400) = 0.2$ radians = 11.5 °. The elastic modulus (E) can be approximated by the bulk modulus of ~ 10 nm anatase particles (230 GPa). [4] According to eq. S9,

$$C_q = \sqrt{\frac{3\times230\times10^9\times(1-\cos 11.5^o)}{\pi\times9.0\times10^9 \sin 11.5^o \times \tan 11.5^o}} = 3.5\ \text{C/m}^2$$

This amount is far beyond the surface charge values of titania (~ 0.1 C/m^2) [5] that can be produced via surface complexation/dissociation in an aqueous solution.

5. Construction and energy minimization of anatase nanocrystal structure models

A single tetragonal bipyramid anatase crystal (ref. Fig. S4C) was constructed by including atoms of anatase (TiO_2, space group $I4_1/amd$) [6] enclosed by 8 {101}-type surfaces, with a face-to-face distance (e.g. between (101) and ($\bar{1}0\bar{1}$)) of nine folds of (101) d-spacing (i.e. 9×3.5166 = 31. 6494 Å). The constructed crystal contains 2907 atoms (969 TiO_2 units) and it is electrically neutral. A truncated bipyramid anatase crystal (as those used for constructing OA structure models in Figs. 3D – 3F and 3J – 3L) was generated be removing atoms on two summits of a formerly constructed bipyramid crystal, exposing two (001) surfaces. Charge neutrality was obtained by manual removal of extra charges (ions) on the surface of the particle.

A linear (straight) anatase nanorod was constructed by perfectly attaching several (non-truncated or truncated) bipyramid anatase crystals on their {101} surfaces (ref. Fig. S4A). The rod elongation direction is approximately [302]. A curved (bent) anatase nanorod was constructed by attaching several bipyramid anatase crystals on their {101} surfaces, with each particle tilted slightly around the [010] axis, with respect to its neighbor (ref. Fig. S4A).

For molecular dynamics (MD) simulations (below) of anatase nanorods constructed above, anatase crystals were described using the interatomic potential functions developed by Matsui and Akaogi.[7] The interaction potential (f_{ij}) between atom i and j is represented by the following equation

$$f_{ij}(r_{ij}) = \frac{q_i q_j}{r_{ij}} + A_{ij}\exp\left(-\frac{r_{ij}}{\rho_{ij}}\right) - \frac{C_{ij}}{r_{ij}^6} \qquad \text{(S10)}$$

The first term accounts for the Coulombic (electrostatic) interaction and the second and third terms for the van der Waals interaction. In the equation, q_i (q_j) is the electrical charge of atom i (j), r_{ij} is the interatomic distance between i and j, and A_{ij}, ρ_{ij} and C_{ij} are model parameters available from ref. 7. The electrostatic interaction is a long-range interaction, i.e. the interaction energy decreases gradually with increasing distance. The van der Waals interaction is a shortrange one, i.e., the interaction energy decreases rapidly and approaches zero at a distance > ~ 10 – 20 Å.

The molecular dynamics (MD) simulation program DL_Poly [8] was used to relax the atomic structure and minimize the crystal energy of a nanorod structure model for subsequent MD simulations. This step reduces the energy gradient with respect to the equilibrium state and helps equilibration in MD at a given temperature (e.g. 300 K). In numerical calculations, the cutoff distances for the Coulombic and van der Waals interactions are important, since they control the accuracy of the calculated energy. To examine the influence of the cutoff distance on the convergence of the calculation, the crystal energy (prior to structure relaxation) was calculated as a function of the cutoff for a straight anatase nanorod shown in Fig. S4A (in which the longest interatomic distance is ~ 300 Å). Results (Table S1) show that in order to obtain a converged energy value, the Coulombic energy cutoff must be no less than 300 Å, the longest interatomic distance in the rod. However, the van der Waals energy cutoff needs only to be ~ 20 Å. This shows that due to the long-range interaction, atomic electrostatic interactions in a nanorod must be calculated using a long energy cutoff. Thus, in this work, both the Coulombic and van der Waals energy cutoffs were set as 400 Å. In computation, such a long energy cutoff significantly increased the computation time for a MD run.

The "zero temperature" MD run method [9] was used to do the energy minimization, which allows gradual atomic motion for structure relaxation at a low temperature (an initial temperature of 1K was set). In a MD run, a time step of 10^{-4} ps was used and it ran to ~ 25 ps when the system energy decreased to a steady value. Figs. S4 and S5 show that, at the steady state, a curved rod has lower crystal energy than a linear one (Figs. S4C and S4D), irrespective of the rod length and (001) faceting (Fig. S5).

As the atomic motions are limited in the low-T MD, after equilibration a system may land in a state with local energy minima. Especially, at a low temperature, the lattice dynamics (thermal vibration of crystal lattices) predominate the motions of a crystal,[10] which is not implemented in the MD program we used. For this, our low-T energy-minimized structures are considered improved initial configurations for later MD simulations at 300 K (below).

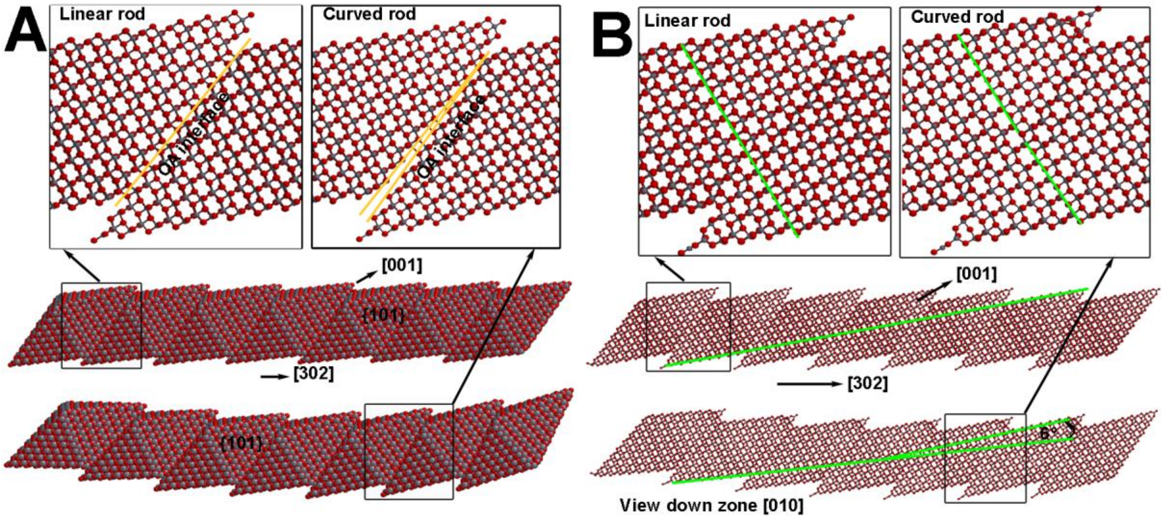

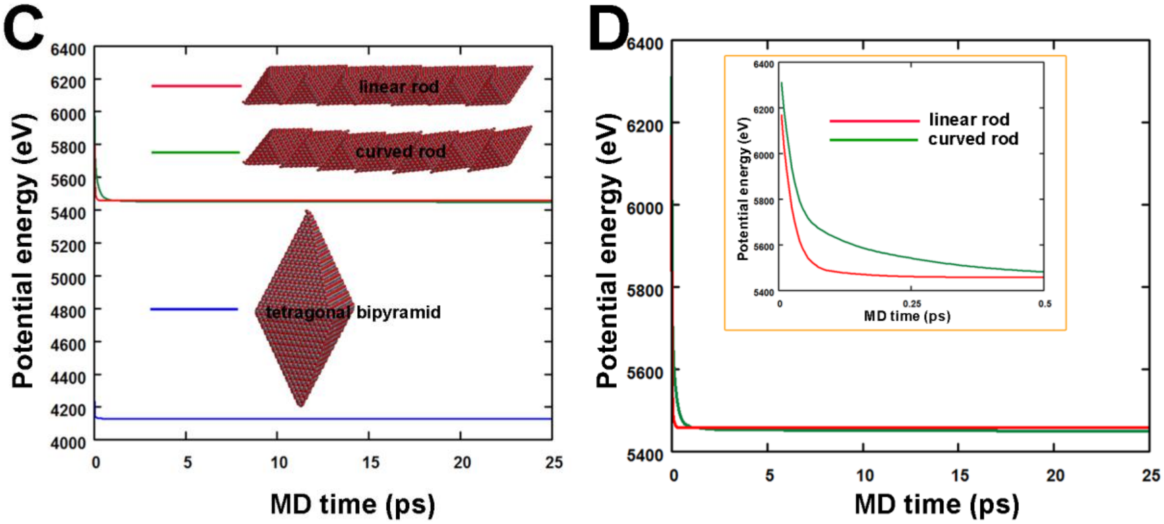

Fig. S4 Structure relaxation and energy minimization of linear and curved anatase nanorods. (**A**) Structure models before energy minimization. (**B**) Structure models after energy minimization. (**C**) Evolution of crystal energy (relative to bulk rutile phase) in energy minimization. For comparison, included is also the energy of a crystal in the tetragonal bipyramid shape from the Wulff construction. (**D**) A closer view of the energy curves of the nanorods in (C). The as-constructed curved rod has a big lattice mismatch in the OA boundary (**A**) and thus higher lattice energy than the linear one (at MD time =0; inset in D). After energy minimization, the lattice mismatch decreased to hardly detectable (**B)**, and the curved rod has a lower lattice energy than the straight one (**C, D**).

Table S1 Influence of energy cutoff on calculated crystal energy of a straight anatase nanorod

Coulombic energy cutoff (Å)	Van der Waals energy cutoff (Å)	Crystal energy (eV)
30	30	-279069.2
50	50	-253700.3
100	100	-269349.7
200	200	-264334.2
300	300	-264506.7
400	400	-264506.8
500	500	-264506.8
400	12	-264487.3
400	15	-264498.8
400	20	-264504.7
400	30	-264506.6
400	40	-264506.8
400	50	-264506.8
400	100	-264506.8
400	200	-264506.8
400	300	-264506.8
400	400	-264506.8

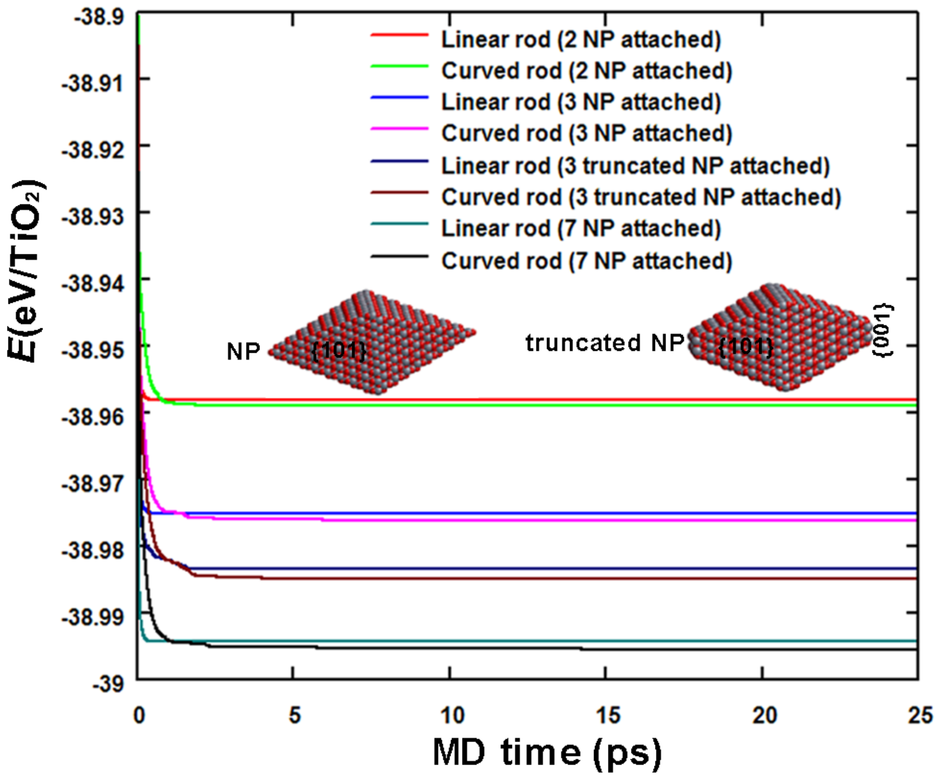

Fig. S5 Minimized crystal energies of linear and curved anatase nanorods formed by attachment of different number of bipyramid nanoparticles (NPs) on their {101} surfaces. Curved rods have lower energies than linear ones; longer rods have lower energies than shorter ones, and rods formed by truncated bipyramid NPs (i.e., with (001) facets) have lower energies than those by bipyramid NPs without truncation (i.e., without (001) facets).

6. Molecular dynamics simulations of anatase nanorods at 300 K

The energy-minimized structures (above) were used as the initial inputs for MD simulations at 300 K using the NVT assemble. The Nose-Hoover algorithm with a relaxation time of 0.1 ps was used for the thermostat. A time step of 10^{-4} ps was used and each MD ran for 65 ps.

In MD, we observed apparent shape oscillation of the curved nanorod formed by OA of 7 bipyramid nanoparticles (Fig. S6). This arises from the deviation of the energy-minimized shape (above) from the true equilibrium shape, as well as the initialization of the velocities of the atoms in the rod at the start of a MD. The two factors combine to drive the shape oscillation. With long-time equilibration, the oscillation should damp to zero and the rod should approach the equilibrium shape.

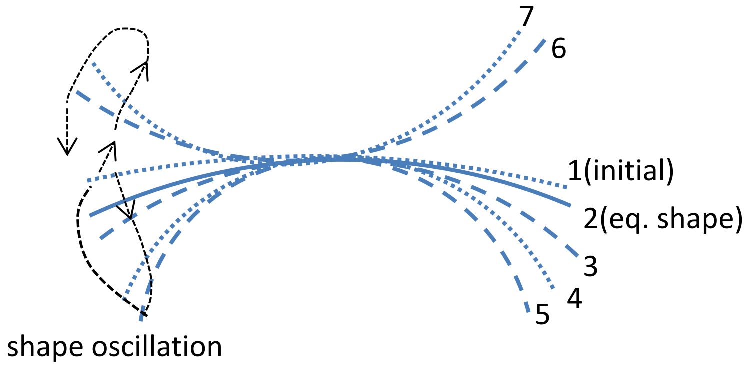

Fig. S6 Schematic of shape oscillation observed in a MD (at 300 K) of a curved anatase rod formed by OA of 7 bipyramid nanoparticles. The initial shape 1 deviates from the equilibrium shape 2. Upon start of the MD, the rod oscillates toward the equilibrium shape. As the assigned initial velocities differ from those at equilibrium, the rod bending overshoots the equilibrium shape 2 and continues to oscillate to shapes 3 and 4, and then reaches the maximum oscillation (shape 5) on one side. Then, the rod oscillates back toward another maximum oscillation shape 7 on the other side. The oscillation continues back and forth until its amplitude damps to zero and the shape converges to the equilibrium one.

7. Structures of anatase nanorods from MD at 300 K

Figure S7 shows sampled structures of anatase nanorods formed by 2 and 3 bipyramid anatase nanoparticles after equilibration by MD at 300 K. All rods are curved, as indicated by the slight misalignment of the lattice fringes in the two terminal nanoparticles, irrespective of the initial (linear or curved) shapes, the number of nanoparticles in OA, and the truncation of the bipyramid vertices that expose {001} faces.

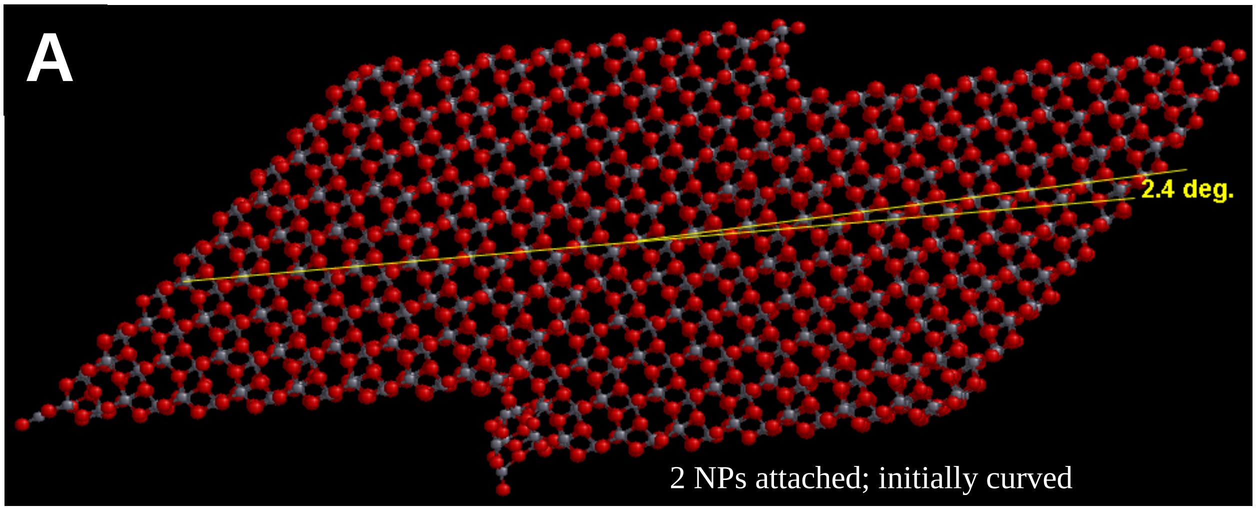

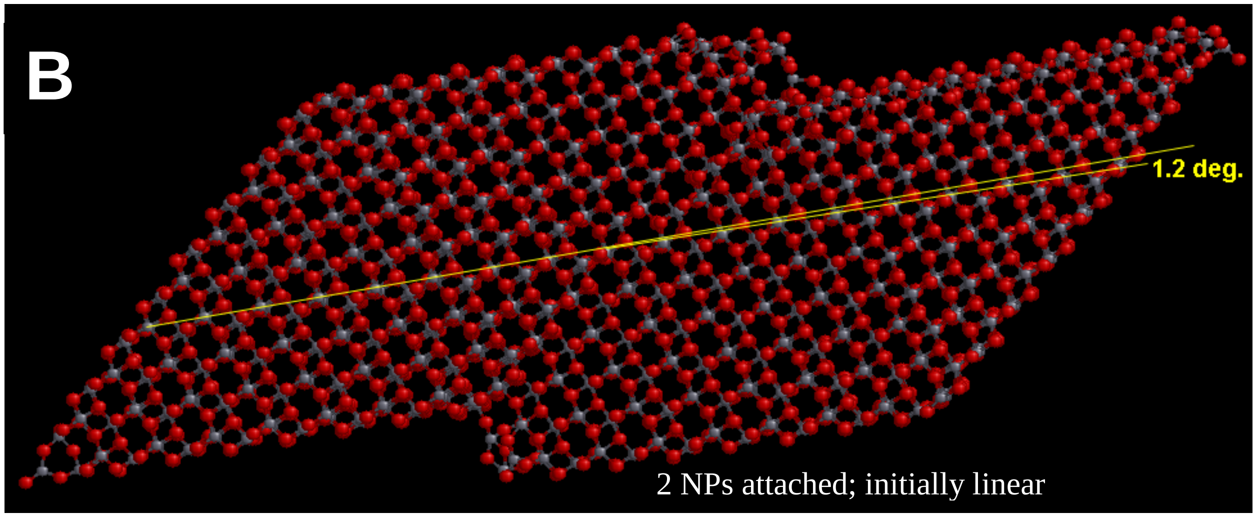
B
1.2 deg.
2 NPs attached; initially linear

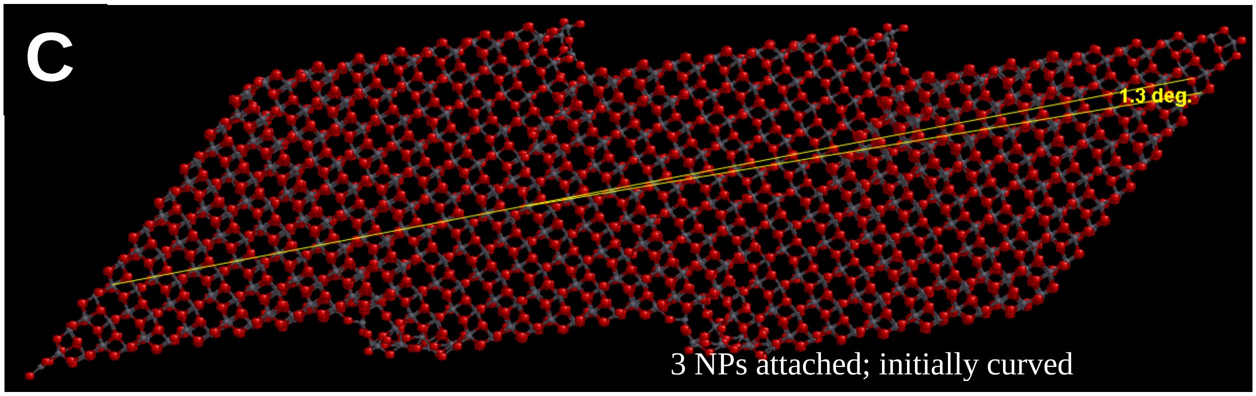
C
1.3 deg.
3 NPs attached; initially curved

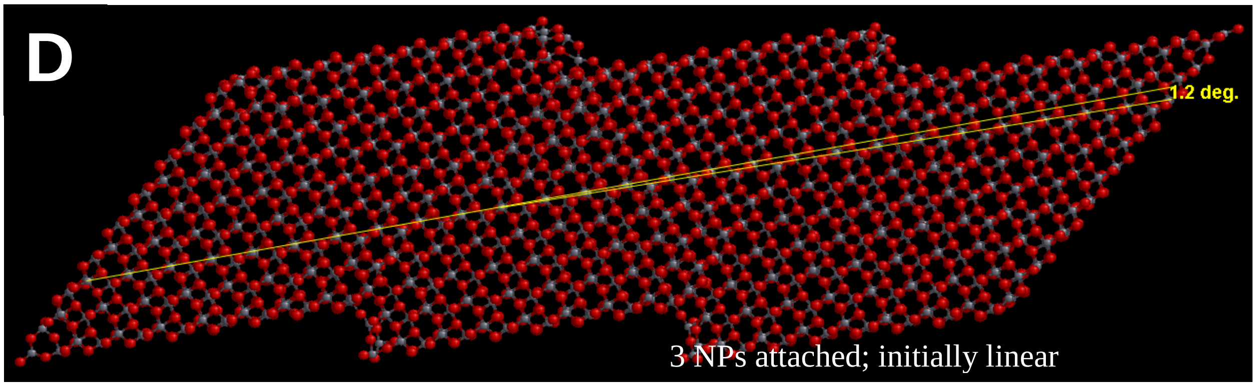
D
1.2 deg.
3 NPs attached; initially linear

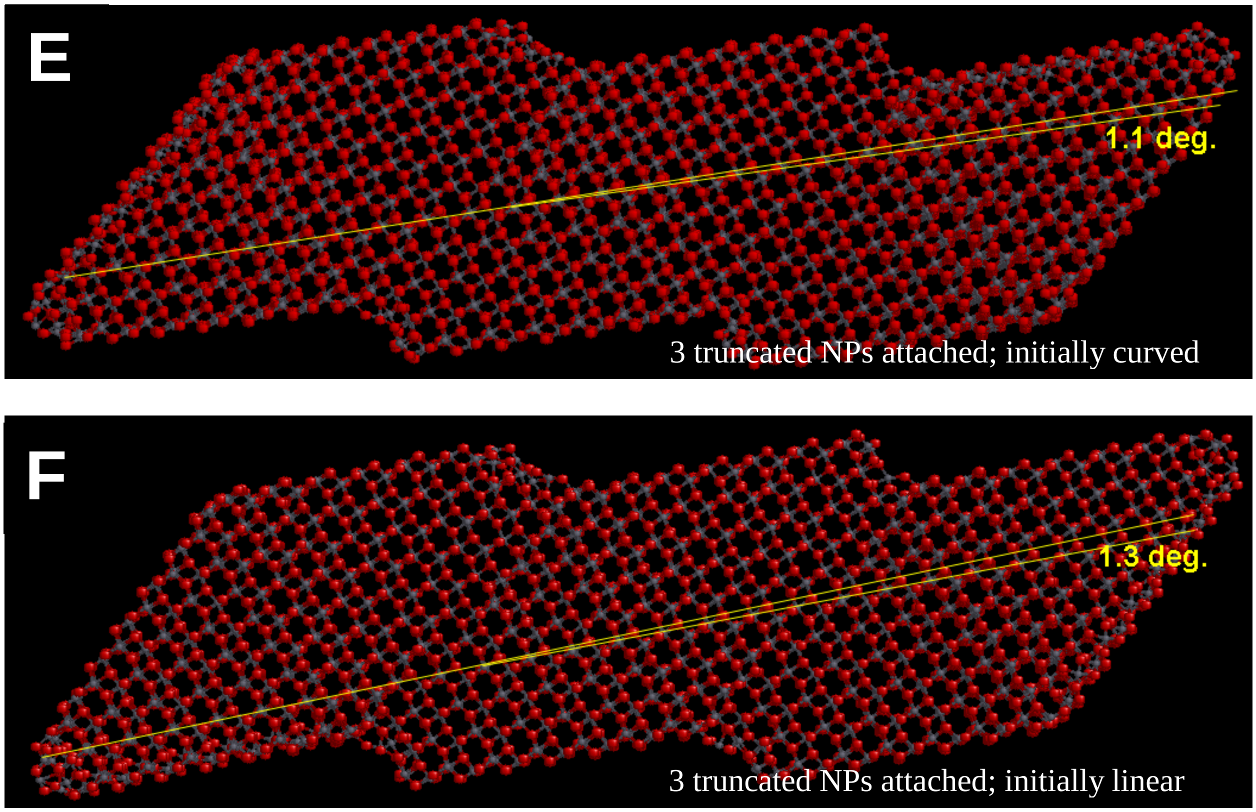

Fig. S7 Snapshots of structures of anatase nanorods at MD time 65 ps. (A) 2 NPs attached; initially curved. (B) 2 NPs attached; initially linear. (C) 3 NPs attached; initially curved. (D) 3 NPs attached; initially linear. (E) 3 truncated NPs attached; initially curved. (F) 3 truncated NPs attached; initially linear. Similar misalignment angles of lattice fringes in initially curved and linear rods (C vs. D; E vs. F) indicate their similar rod curvatures.

References

1. K. Bourikas, T. Hiemstra and W. H. Van Riemsdij, *Langmuir*, 2001, **17**, 749–756.
2. H. Zhang and J. F. Banfield, *J. Phys. Chem. B*, 2000**, 104**, 3481–3487.
3. F. Ullmann, *Ullmann's Chemical Engineering and Plant Design, Vol.*1, Wiley-VCH, Weinheim, 2005.
4. B. Chen, H. Zhang, K. A. Dunphy-Guzman, D. Spagnoli, M. B. Kruger, D. V. S. Muthu, M. Kunz, S. Fakra, J. Z. Hu, Q. Z. Guo and J. F. Banfield, *Phys. Rev. B*, 2009, **79**, 125406.
5. M. P. Finnegan, H. Zhang and J. F. Banfield, *J. Phys. Chem. C*, 2007, **111**, 1962–1968.

6. FIZ Karlsruhe – Leibniz Institute for Information Infrastructure, *Inorganic Crystal Structure Database (ICSD/Retrieve* v.2.01), Karlsruhe, 1997 (File No. 202242).

7. M. Matsui and M. Akaogi, *Molecular Simulation*, 1991, 6, 239–244.

8. I.T.Todorov, W. Smith, K. Trachenko and M. T. Dove, *J. Mater. Chem.*, 2006, **16**, 1911 – 1918.

9. I. T. Todorov and W. Smith, *The DL_Poly_3 (v.3.06) User Manual*, CCLRC Daresbury Laboratury, Cheshire, UK, 2006.

10. J.D. Gale, *General Utility Lattice Program (v.3.4)*, Curtin University of Technology, Perth, Australia.